

A new fission-fragment detector to complement the CACTUS-SiRi setup at the Oslo Cyclotron Laboratory

T.G. Tornyi^{a,b,*}, A. Görgen^a, M. Guttormsen^a, A.C. Larsen^a, S. Siem^a,
A. Krasznahorkay^b, L. Csige^{b,c}

^a*Department of Physics, University of Oslo, Norway*

^b*Institute of Nuclear Research of the Hungarian Academy of Sciences (MTA Atomki), Debrecen, Hungary*

^c*Max-Planck-Institute for Quantum Optics, D-85748 Garching, Germany*

Abstract

An array of Parallel Plate Avalanche Counters (PPAC) for the detection of heavy ions has been developed. The new device, NIFF (Nuclear Instrument for Fission Fragments), consists of four individual detectors and covers 60% of 2π . It was designed to be used in conjunction with the SiRi array of $\Delta E - E$ silicon telescopes for light charged particles and fits into the CACTUS array of 28 large-volume NaI scintillation detectors at the Oslo Cyclotron Laboratory. The low-pressure gas-filled PPACs are sensitive for the detection of fission fragments, but are insensitive to scattered beam particles of light ions or light-ion ejectiles. The PPAC detectors of NIFF have good time resolution and can be used either to select or to veto fission events in in-beam experiments with light-ion beams and actinide targets. The powerful combination of SiRi, CACTUS, and NIFF provides new research opportunities for the study of nuclear structure and nuclear reactions in the actinide region. The new setup is particularly well suited to study the competition of fission and γ decay as a function of excitation energy.

Keywords: PPAC, fission fragment detector, coincidence

PACS: 29.40.-h

1. Introduction

In-beam spectroscopy of heavy nuclei often requires the detection of fission fragments, either because the fission process itself or the fission fragments are to be investigated, or to study alternative decay processes where fission events need to be suppressed as unwanted background. Cross sections for nuclear reactions induced by neutrons or light charged particles on actinide nuclei are important for nuclear energy applications and their measurements usually require the detection of fission fragments. It is often difficult or even impossible to directly measure cross sections of neutron-induced reactions on short-lived actinides because the radioactivity of the target sample would be prohibitively large. A surrogate method using charged-particle induced reactions to produce the same excited compound nucleus from a longer-lived target nucleus was originally proposed by Cramer and Britt [1] and is now regularly used [2]

*Corresponding author.
Prepared for submission to *Physica Scripta* from atomki.hu (T.G. Tornyi)

23 to study the decay of the compound nucleus, which is thought to be independent of its
24 production mechanism.

25 The Oslo Cyclotron Laboratory (OCL) at the University of Oslo hosts the highly
26 efficient CACTUS array [3] of large-volume NaI scintillation detectors coupled to the
27 SiRi array [4] of silicon $\Delta E - E$ detector telescopes. CACTUS consists of 28 $5'' \times 5''$
28 NaI detectors with a full-energy peak efficiency of 15% at 1.3 MeV. Each scintilla-
29 tor is placed at a distance of 22 cm from the target and mounted with a 10 cm thick
30 conical lead collimator with an opening of $\varnothing = 70$ mm at the front surface. The CAC-
31 TUS array can be complemented by high-purity germanium detectors and large-volume
32 $\text{LaBr}_3(\text{Ce})$ scintillator detectors.

33 The SiRi particle telescope system [4] comprises eight trapezoidal modules ar-
34 ranged in a lampshade geometry facing the target at a distance of 5 cm at an angle
35 of 45° . Each telescope module consists of a $130 \mu\text{m}$ thick silicon detector in the front
36 and a $1550 \mu\text{m}$ thick back detector allowing particle identification via $\Delta E - E$ mea-
37 surements. The front detectors are segmented into eight curved strips, which allows
38 measuring the scattering angle of the light-ion projectile with a resolution of 2° . SiRi
39 can either be mounted in forward direction covering scattering angles θ between 40
40 and 54° , or in backward direction covering angles between 126 and 140° . In experi-
41 ments using direct reactions with proton, deuteron, ^3He , or ^4He beams from the Oslo
42 Cyclotron, the detection of the charged ejectiles in SiRi provides a measure of the excita-
43 tion energy of the binary reaction partner with a typical energy resolution of 150 keV .

44 The combination of the SiRi-CACTUS setup with an efficient fission-fragment de-
45 tector array is well suited for cross section measurements using the surrogate tech-
46 nique. A compact fission detector inside the CACTUS array also offers the possibility
47 to perform other types of experiments where either a tag on fission events or a veto is
48 required. In addition to fitting into the CACTUS array, it was a requirement that the
49 new fission fragment detector can be used together with the SiRi charged-particle tele-
50 scopes, which limited the angular coverage to only one hemisphere. For this purpose a
51 fission fragment detector based on Parallel Plate Avalanche Counters (PPAC) was built.
52 In this paper we present the design and discuss the performance of the new detector.

53 2. Design parameters

54 The most important design parameter for the new detector was a high detection
55 efficiency for fission fragments. Energy and position resolution are not important for
56 the purpose of a pure tagging or veto detector. To allow the measurement of triple
57 coincidences between light charged particles, γ -rays, and fission fragments, the fission
58 fragment detectors should be fast with a time resolution of the order of nanoseconds.
59 Ideally the detector should only trigger on heavy ions and be insensitive to light ions,
60 electrons, and γ -rays. Given these requirements we have chosen to base the new de-
61 tector on low-pressure gas filled PPAC [5, 6, 7, 8, 9, 10]. It is a further advantage that
62 PPAC detectors do not show ageing effects due to the continuous exchange of the gas,
63 contrary to silicon detectors, for example, which would rapidly deteriorate with heavy-
64 ion implantation. A fission-fragment detector based on PPAC detectors requires only
65 small amounts of material inside the vacuum chamber, having no significant influence
66 on the performance of the CACTUS detectors due to scattering of γ -rays.

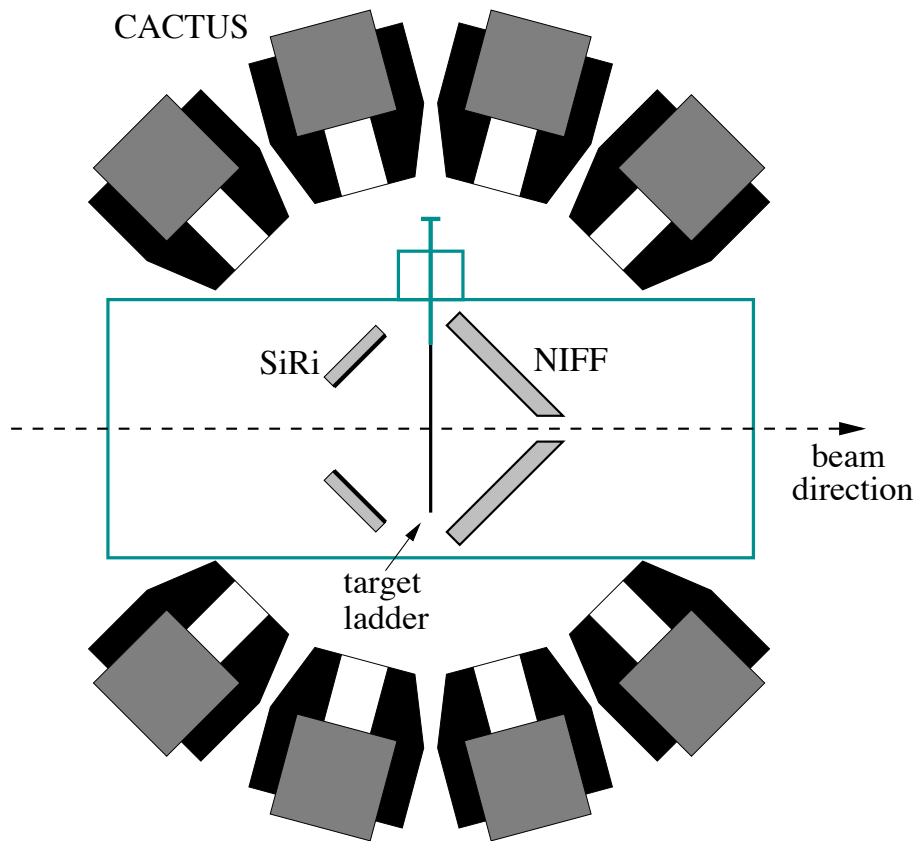


Figure 1: Schematic view (not to scale) of the setup comprising the CACTUS array of 28 collimated NaI detectors surrounding the vacuum chamber with the SiRi particle telescope array mounted under backward angles and the new NIFF fission-fragment detector under forward angles. Targets are inserted into the space between SiRi and NIFF via a target ladder.

67 The design parameters of the PPAC detectors were strongly limited by the geome-
68 try and the size of the existing setup comprising CACTUS and SiRi. The geometry of
69 the setup is shown schematically in Fig. 1. Since the silicon telescopes of SiRi together
70 with their support structure cover either the forward or backward hemisphere with re-
71 spect to the beam direction, only one hemisphere is available for the fission-fragment
72 detector. Since the aim of the detector is to determine whether fission occurred or not,
73 it is sufficient to detect only one of the two fission fragments, which are emitted in
74 opposite direction in light-ion induced reactions. In this way it is possible to achieve
75 high efficiency although less than 50% of the solid angle is covered.

76 The NaI detectors of CACTUS are mounted at fixed positions and their collimators
77 leave a cylindrical space for the target chamber, which has an inner diameter of 11.7 cm
78 and a length of 48.0 cm. A new chamber was designed that allows inserting a target
79 ladder from the side into the space between SiRi and the fission detector, replacing the
80 previously used rotating target changing system. The PPAC detectors were designed
81 to cover the largest possible fraction of the forward hemisphere. However, an opening
82 is needed to allow the beam to exit, and it is not necessary to cover angles close to
83 90° with respect to the beam axis, since the fission fragments that are emitted in this
84 direction lose all their energy in the target or the target frame. The NIFF detector
85 consists of four PPAC modules which are arranged like the leaves of a four-leaf clover,
86 as illustrated in Fig. 2. Each module has an overall length of 62.5 mm and an overall
87 width of 77 mm, where the outer part forms a sector of a circle with 44.5 mm radius.
88 The modules are placed at an angle of 45° with respect to the beam axis. A square of
89 20 mm side length in the center of the detector allows the beam to exit. The active area
90 of NIFF covers $\sim 60\%$ of the forward hemisphere. Measurements with a ^{252}Cf source
91 and the performance of the detector are discussed in Sect. 6.

92 3. Detector Layout

93 Each PPAC module consists of three main parts: an entrance window, the cathode
94 foil, and the anode plate. The layout of the PPAC modules is shown in Fig. 2. Both
95 the entrance window and the cathode foil are made of $1.5\ \mu\text{m}$ thick Mylar foil, which
96 is aluminised on one side. The thin aluminium layer is necessary to avoid the build-
97 up of charge on the foils, which are coupled to ground potential (see Figure 4). The
98 backplate of the PPAC modules is made from a single-sided printed-circuit board, with
99 the polished copper layer of the sheet acting as anode of the PPAC. The modules are
100 filled with high-purity ($> 99.95\%$) isobutane (C_4H_{10}) gas at low pressure as the active
101 material of the detector. The anode back-plate of each PPAC module has two holes
102 of 2 mm diameter fitted with a small copper tube through which the gas enters and
103 exits. The four modules are chained together with silicone tubing. In this way the gas
104 is flowing subsequently through all four modules. The cathode foil is held by a PVC
105 frame at a distance of 3.5 mm from the anode plate.

106 The pressure difference between the gas inside the PPAC module and the vacuum of
107 the target chamber would cause the cathode foil to bulge outward. To obtain a uniform
108 efficiency the cathode foil must be parallel with the anode back plate. To achieve this,
109 a second, identical foil is placed on top of the cathode foil at a distance of 2 mm using
110 a second PVC frame. The volumes between the two Mylar foils and between the cathode

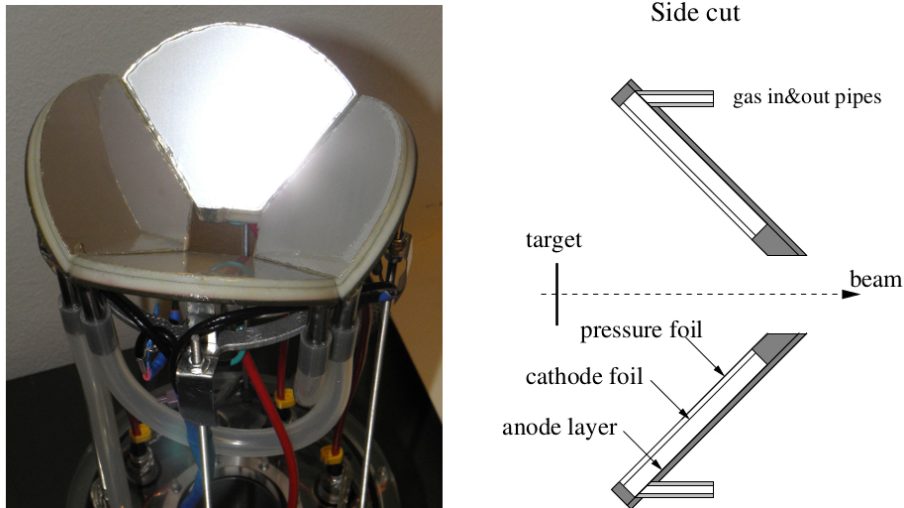


Figure 2: Photo and cross section of NIFF detector. The dimensions of the PPAC modules and their arrangement are described in the text.

111 foil and anode back plate are connected via a small hole in the frame. In this way only
 112 the outer foil bulges outward, while the cathode foil remains parallel with the anode.
 113 The frames that hold the Mylar foils in place have a width of 3 mm, forming a 3 mm
 114 wide rim around each module that is insensitive to fission fragments. The total active
 115 area for each PPAC module is approximately 2240 mm².

116 4. Gas Control System

117 During operation the avalanche process leads to polymerization of the isobutane
 118 gas, which affects the detection efficiency of the PPAC modules. It is therefore nec-
 119 essary to replace the gas continuously in order to maintain a high efficiency that is
 120 constant over time. The four PPAC modules are chained together with the gas flowing
 121 subsequently through all four modules. A continuous gas flow of ≈ 1 ml/s is necessary
 122 to maintain a good efficiency. At the same time the pressure inside the PPAC modules
 123 has to be kept constant to avoid fluctuations of the detection efficiency. This is achieved
 124 by the gas control system shown in Fig. 3.

125 The pressure inside the detector loop is measured with an MKS 626B Baratron
 126 absolute capacitance manometer and maintained at a constant value by an MKS 250E
 127 gas inlet pressure controller. During operation the gas is continuously pumped out from
 128 the detector loop through a needle valve. If the pressure falls below a lower threshold
 129 the inlet controller opens an MKS 248A control valve until the pressure reaches an
 130 upper threshold. In this way the pressure is kept constant within a preset range. A
 131 typical pressure inside the PPAC modules is ≈ 5 mbar, which is kept within a range of
 132 $\approx 2\%$. The gas flow is adjusted by opening or closing the needle valve.

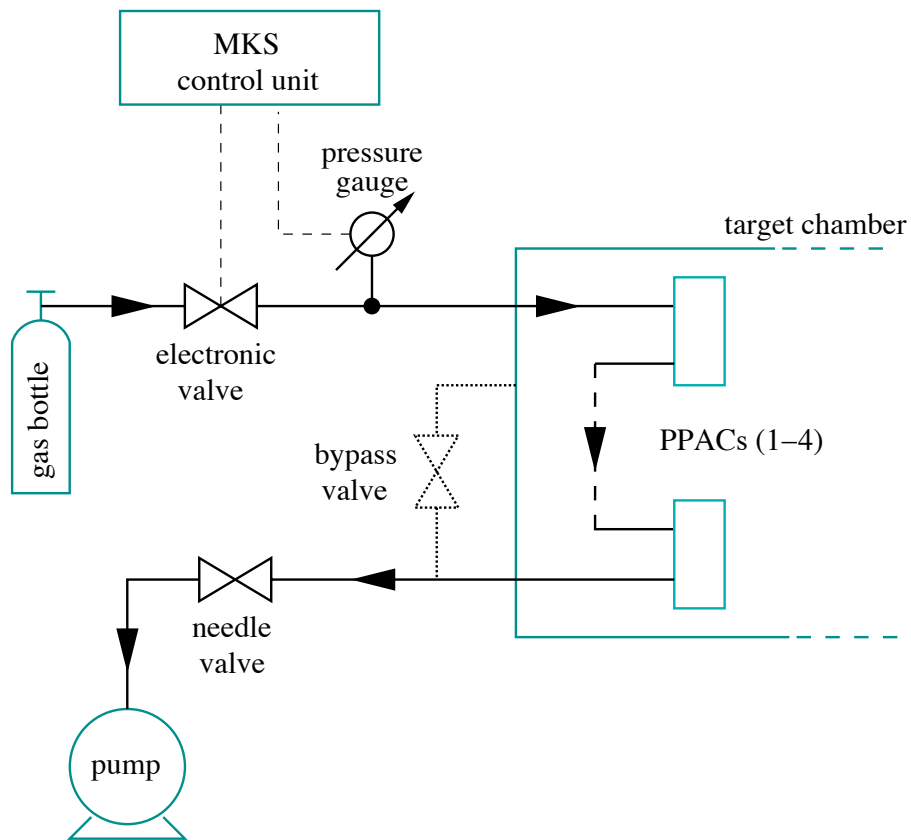


Figure 3: Schematic drawing of the gas control system that keeps the pressure inside the PPAC modules constant and at the same time maintains a steady flow of isobutane gas.

133 Particular care has to be taken when evacuating or venting the target chamber. The
 134 detector volume is separated from the volume of the target chamber only by the 1.5 μm
 135 thick Mylar foil, which will easily be damaged when the pressure difference becomes
 136 too large. Tests have shown that the foils can withstand a pressure difference of 10 mbar
 137 without damage. A bypass valve is used to connect the detectors with the volume of
 138 the target chamber. In this way both volumes can be pumped down simultaneously
 139 before the detectors are filled with isobutane. Conversely, the gas from the detectors
 140 can be vented into the chamber vacuum through the bypass valve before both volumes
 141 are brought up to atmospheric pressure simultaneously.

142 5. Electronics and Data Acquisition

143 A schematic drawing of the detector system and the signal processing electronics
 144 is shown in Fig. 4. To avoid the build-up of charge, both the entrance windows and

145 cathode foils are connected to a common ground. A common positive high voltage of
146 ≈ 400 V is applied to the anodes via $1\text{ M}\Omega$ resistors. The resistors, together with a 2 nF
147 coupling capacitor to ground, prevent cross-talk between the four different detector
148 modules. The fission fragments enter the active detector volume through the entrance
149 window and cathode foil and ionize the isobutane gas along their trajectory. The elec-
150 trostatic field accelerates the primary electrons towards the anode. If the voltage is high
151 enough the primary electrons create an avalanche of secondary electrons in collisions
152 with the gas. The avalanche effect provides sufficient charge on the anode to produce
153 a measurable signal, which is taken out via 2 nF capacitors to decouple the preampli-
154 fier input from the high voltage. The detector performance was tested as a function
155 of isobutane gas pressure in the detector and as a function of the applied high voltage.
156 The results are described in Sect. 6.

157 The anode signals pass through Ortec VT120A fast preamplifiers with a gain factor
158 of 200, which are located on the outside of the target chamber in close proximity
159 to the vacuum feedthroughs. The signals are further amplified using Tennelec TC248
160 shaping amplifiers. The fast output signals are fed into an Ortec CF8000 constant
161 fraction discriminator. The logic signal of the CFD output is used in the VME-based
162 data acquisition system [4] to determine the time difference between the detection of
163 a fission fragment in NIFF and a light charged particle in the SiRi telescopes, which
164 generates the event trigger. The pulse height of the PPAC contains no information and
165 is not used in the data processing.

166 6. System performance

167 The performance of the new PPAC detectors was first tested using a ^{252}Cf source
168 and its integration with the SiRi charged-particle telescopes and the CACTUS array of
169 NaI scintillation detectors was tested during in-beam experiments with ^{238}U and ^{237}Np
170 targets.

171 A ^{252}Cf source of well-known activity was used to measure the efficiency of the
172 individual PPAC modules and the detector as a whole. The count rates of the individual
173 PPAC modules were found to be very similar to each other and within 4% of the average
174 count rate of the four modules during both source and in-beam measurements. The test
175 with the ^{252}Cf source showed that the PPAC modules only trigger on fission fragments,
176 which originate from the 3.09% spontaneous fission branch, but not on the 6.1 MeV α
177 particles from the predominant α -decay branch.

178 The efficiency of the total detector array to detect fission fragments was measured
179 as a function of the isobutane gas pressure inside the PPAC modules and as a function
180 of the applied high voltage. The ^{252}Cf source was mounted at the target position for
181 this measurement. The results of the measurement are shown in Fig. 5. The statistical
182 uncertainty of the individual measurements is better than 1%. The curves indicate
183 the optimum voltage for a given gas pressure. Once the plateau region is reached,
184 the efficiency increase with pressure and voltage is very small. To avoid damage of
185 the thin entrance windows the detectors were only operated with gas pressures below
186 5 mbar. The detectors are furthermore insensitive to light charged particles at such low
187 pressure. Within this limit the highest efficiency for the detection of fission fragments
188 was found for a gas pressure of 5 mbar and a voltage of 400 V. These parameters were

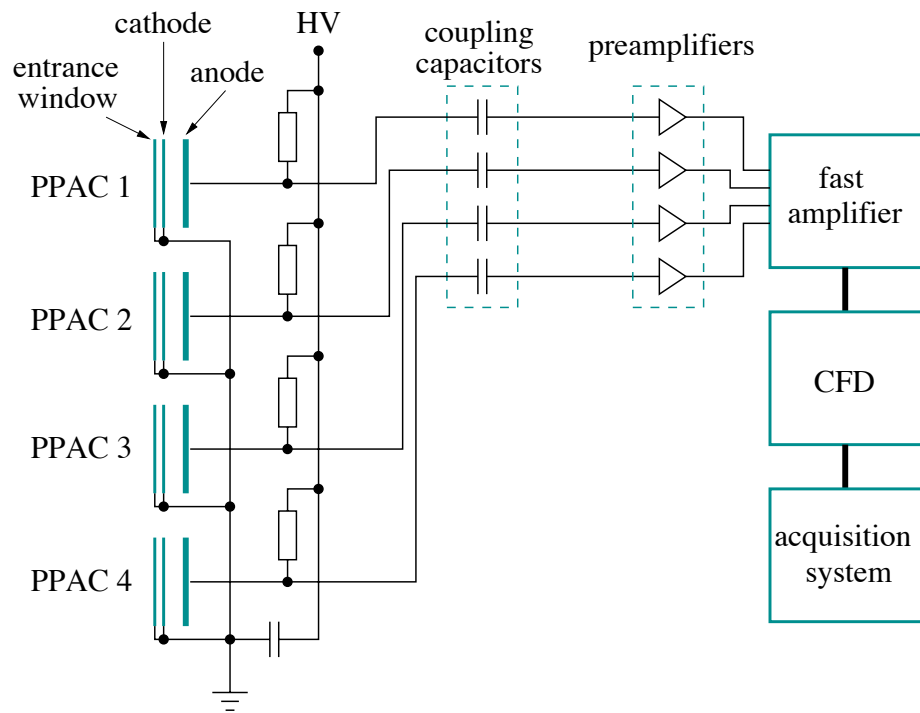


Figure 4: Since anodes are fed by one high voltage supply, resistances and a coupling capacitor to the ground are needed to prevent electronic crosstalk.

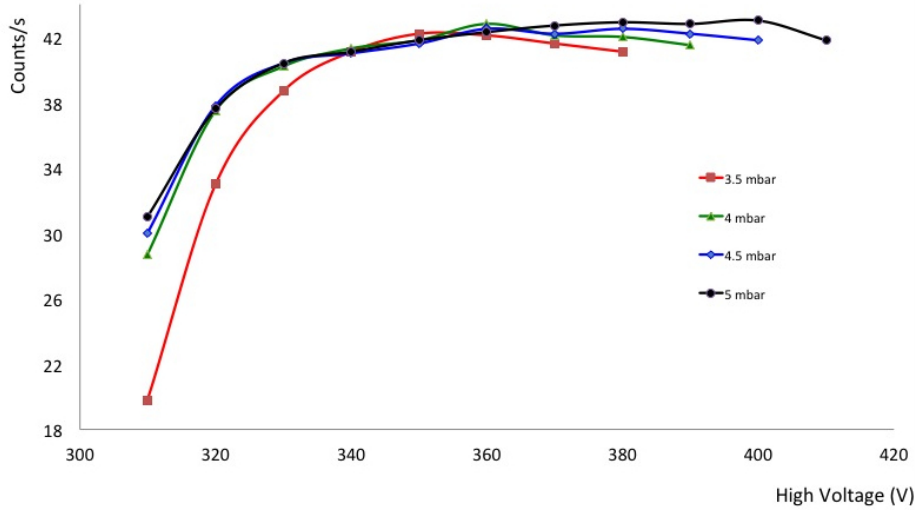


Figure 5: Count rates of the total PPAC detector array as a function of high voltage for different isobutane gas pressures. A ^{252}Cf source of well-known activity was placed at the target position of the chamber. The statistical uncertainty of the individual data points is less than 1%.

189 chosen for all subsequent measurements. Fig. 5 also illustrates that pressure variations
 190 of the order of 2% (cf. sect. 4) have negligible implications for the efficiency of the
 191 detectors. Under these conditions the four PPAC modules counted fission fragments
 192 at a total rate of 43.2(4) Hz. The activity of the source was derived from a previous
 193 measurement of the α activity and, taking into account the half-life of ^{252}Cf , an activity
 194 of 2.54(8) kBq was determined. With a fission branch of 3.09% we find the fission rate
 195 to be 78.5(24) Hz. From the decay rate we determine the probability to detect fission
 196 events in NIFF to be 55(2)%. We have estimated that the active areas of the four PPAC
 197 modules cover just under 60% of the forward hemisphere, which corresponds to the
 198 chance that one of the two fission fragments enters the active volume of the detector.
 199 We can therefore conclude that the intrinsic efficiency of the PPAC modules to detect
 200 an incoming fission fragment is well above 90%.

201 After the extensive measurements with the ^{252}Cf source the new detector was also
 202 tested during an in-beam experiment using the reaction $^{238}\text{U}(\text{d},\text{p})\text{f}$. The deuteron beam
 203 energy was 12 MeV and the metallic ^{238}U target had a thickness of 260 $\mu\text{g}/\text{cm}^2$. The
 204 data acquisition was triggered by the logic OR of the back detectors of SiRi. The energy
 205 information from the thin ΔE front detectors and the thick back detectors are used to
 206 identify the charged-particle ejectiles which are detected in the SiRi telescopes under
 207 backward angles, essentially protons, deuterons, and tritons. Almost all fission frag-
 208 ments that are detected in the PPAC modules of NIFF are associated with low-energy
 209 protons detected in SiRi, *i.e.* the fragment originates from the fission of ^{239}U above the
 210 threshold. The spectrum in Fig. 6 shows the time difference between the detection of a

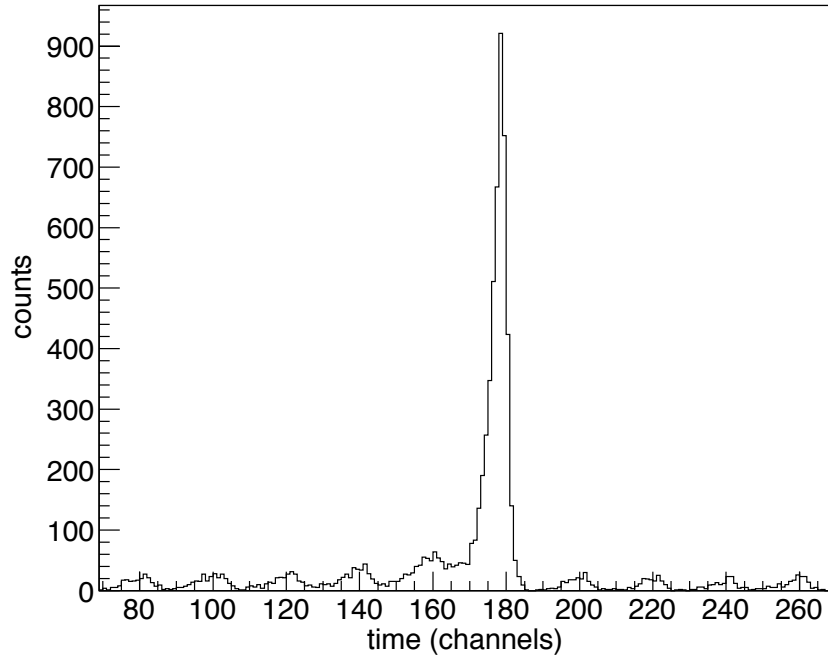


Figure 6: Spectrum showing the time difference between particles detected in SiRi (start signal) and fission fragments detected in NIFF (stop signal) taken during an in-beam measurement with the reaction $^{238}\text{U}(\text{d},\text{pf})$ at a beam energy of 12 MeV. The smaller peaks correspond to random coincidences between different beam bursts. Each channel on the abscissa corresponds to a time interval of 2.4 ns.

211 proton in SiRi, which provides the start signal, and the detection of a fission fragment
 212 in one of the PPAC modules, which provides the stop signal. The peak has a width of
 213 11 ns FWHM, which is typical for the silicon detectors of SiRi. Fast signal rise times
 214 observed for the PPAC modules suggest that the NIFF detectors are fast compared to
 215 the silicon detectors and that the time resolution is entirely dominated by the SiRi de-
 216 tectors. It would in principle be possible to operate the PPAC detectors with count rates
 217 in the MHz region. However, in experiments where NIFF is coupled to SiRi and CAC-
 218 TUS the count rates are usually limited by the latter and are not expected to exceed a
 219 few kHz in NIFF.

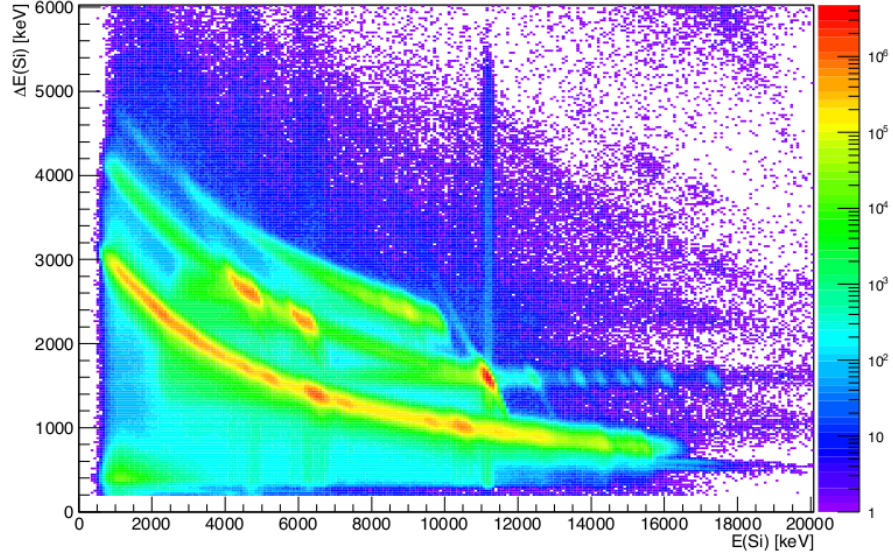
220 The new PPAC detector was furthermore tested in another in-beam experiment with
 221 the reaction $^{237}\text{Np}(\text{d},\text{pf})$. In this case the deuteron beam energy was 13.5 MeV and the
 222 target consisted of ^{237}Np oxide with a thickness of $200\ \mu\text{g}/\text{cm}^2$ on a $20\ \mu\text{g}/\text{cm}^2$ thick
 223 carbon backing. The target contained a total amount of $35\ \mu\text{g}$ of ^{237}Np and had an α
 224 activity of 0.9 kBq. As was the case for the source measurement with ^{252}Cf , the α

225 particles from the decay of ^{237}Np do not ionize the isobutane gas sufficiently for the
226 PPAC detectors to give any signals. The decay α particles are furthermore stopped in
227 the ΔE front detectors of SiRi. Without reaching the back detectors of the telescopes
228 they do not trigger the data acquisition, and all recorded events are due to deuteron-
229 induced reactions on the target.

230 The spectra of Fig. 7 show $\Delta E - E$ particle identification plots from the $d+^{237}\text{Np}$
231 experiment. The upper spectrum contains all events recorded in SiRi without any condi-
232 tion on the NIFF fission fragment detector. Three distinct curves are observed that are
233 associated with (bottom to top) protons, deuterons, and tritons. The strongest peak at
234 the highest deuteron energy is due to elastic scattering of the projectiles on ^{237}Np . The
235 other strong peaks associated with detected deuterons are due to elastic scattering on
236 ^{16}O and ^{12}C , respectively. The strong peaks associated with detected protons are due
237 to inelastic scattering to excited states in ^{16}O and ^{12}C . The lower spectrum shows the
238 same particle-identification plot with the condition that a fission fragment was detected
239 in NIFF. As can be seen, fission events are associated with the detection of protons
240 of a certain energy range. The few events where fission was detected together with
241 deuterons (note the logarithmic scale) are due to random coincidences. Reactions in
242 which protons are emitted with the maximum energy of $\sim 16\text{MeV}$ leave ^{238}Np in the
243 ground state. The lower the energy of the ejectile the higher is the excitation energy
244 of the reaction product. Fission is observed for proton energies lower than $\sim 10\text{MeV}$,
245 which corresponds to an excitation energy of $\sim 6\text{MeV}$ and coincides with the fission
246 threshold in ^{238}Np . The example illustrates how the new NIFF detector can be used
247 to determine fission cross sections and the shape of the fission barrier for more exotic,
248 less-known actinide isotopes.

249 The detection of fission fragments in NIFF allows identifying γ -rays that are asso-
250 ciated with the fission process. Fig. 8 shows γ -ray spectra as a function of excitation
251 energy for ^{238}Np . In a first step proton events were selected in the $\Delta E - E$ identification
252 matrix. Next a time gate was applied to select γ -rays that were recorded in CACTUS in
253 prompt coincidence with the protons. The excitation energy of the nucleus can be de-
254 termined from the measured proton energy and the reaction kinematics. In this way it is
255 possible to extract the γ -ray spectrum for a given bin of excitation energy in ^{238}Np [11].
256 The resulting two-dimensional spectrum is shown in Fig. 8 on the top. A few discrete
257 γ -ray transitions are clearly visible. These originate from excited states in ^{13}C and ^{17}O ,
258 which are populated in (d,p) reactions on the carbon backing and oxygen in the target,
259 and can be easily subtracted. The lower part of Fig. 8 shows the same data set with the
260 additional condition that a fission fragment was detected in NIFF. From these spectra
261 it is possible to extract information on the competition between γ decay and fission as
262 a function of excitation energy. Under the assumption that the formation and decay of
263 a compound nucleus are independent of each other, such measurements can be used
264 to determine cross sections for compound nuclear reactions via the so-called surrogate
265 method. The technique is particularly useful in cases where the direct measurement of
266 (n, γ) and (n,f) cross sections is not feasible because the required actinide targets are
267 too short-lived.

ΔE : E for all detectors together



ΔE : E in coincidence with fission

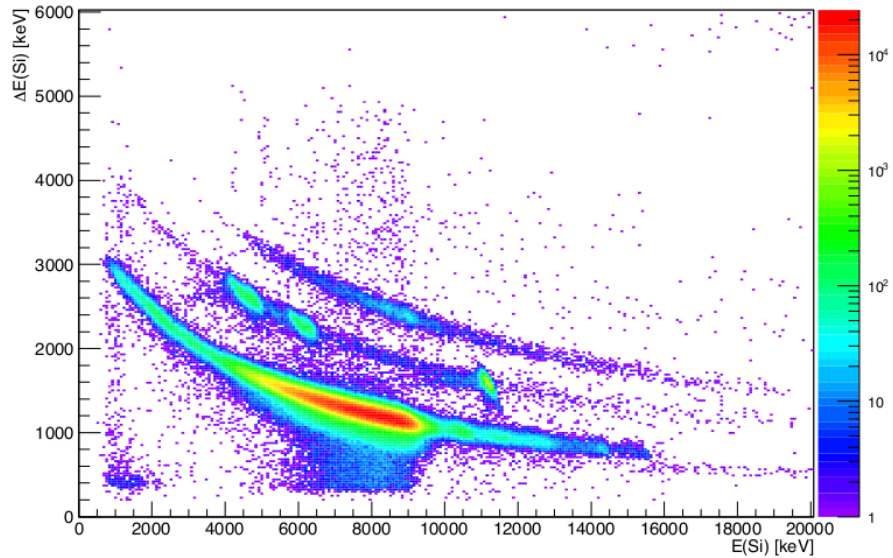


Figure 7: Particle identification plots showing the energy loss ΔE in the front detectors of SiRi versus the total energy E of the particles ejected following the $d+^{237}\text{Np}$ reaction. The upper spectrum shows all recorded events, the one on the bottom only those that were recorded in coincidence with a fission fragment in NIFF. The three separate loci visible in the total identification plot correspond to (bottom to top) protons, deuterons, and tritons. Fission events are only associated with protons below a certain energy, which corresponds to fission of ^{238}Np above the fission threshold.

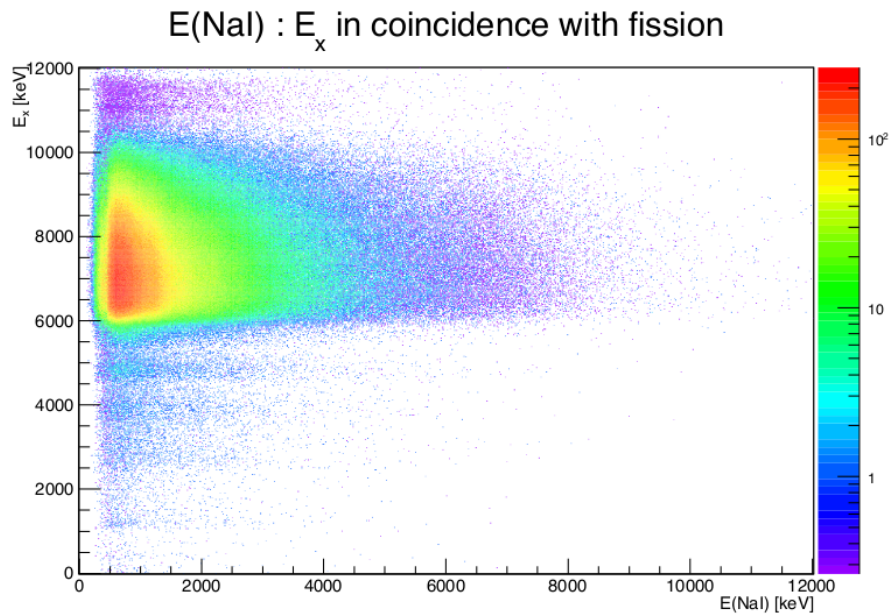
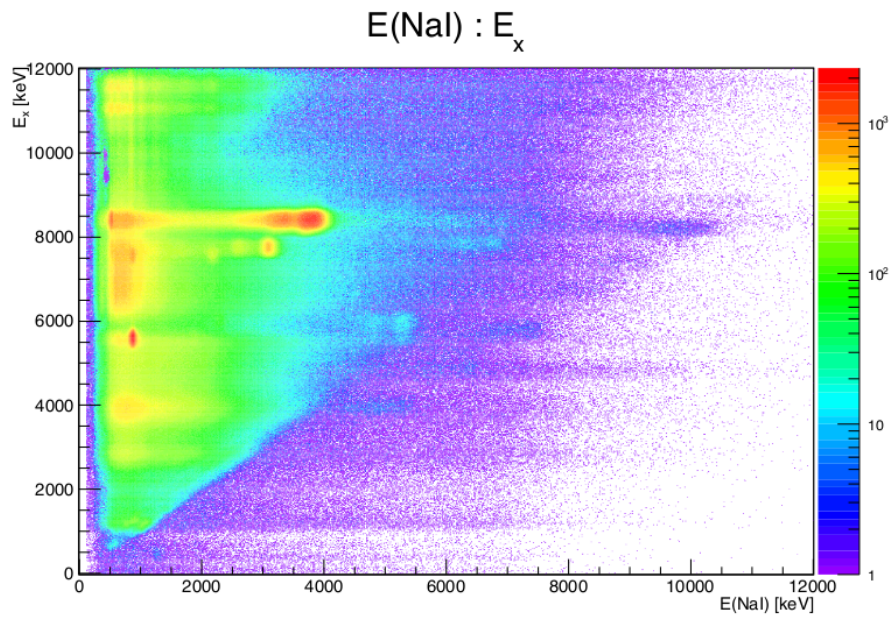


Figure 8: Excitation energy versus γ -energy matrices for the reaction $^{237}\text{Np}(d,p)^{238}\text{Np}$. The excitation energy is obtained from the measured kinetic energy of the protons and the reaction kinematics. The spectrum on the bottom was obtained with the additional condition that a fission fragment was detected in the NIFF detector in coincidence with a proton in SiRi and γ -rays in CACTUS.

268 7. Conclusion

269 A new fission fragment detector based on parallel-plate avalanche counters was
270 developed at the University of Oslo. It was designed to be used inside the CACTUS
271 array of large-volume NaI scintillation detectors together with the SiRi charged-particle
272 telescope array. The new detector consists of four PPAC modules which cover close
273 to 60% of the forward hemisphere. The efficiency of the detector was measured with
274 a ^{252}Cf source. The intrinsic efficiency for heavy ions was found to be well above
275 90%, resulting in an efficiency for the detection of one of the two fragments from a
276 fission event of 55(2)%. The PPAC detectors are insensitive to light ions, electrons,
277 neutrons, or photons. The integration of the fission detector into the existing CACTUS
278 and SiRi data acquisition system was tested during in-beam experiments with deuteron
279 beams and ^{238}U and ^{237}Np targets. The detector has excellent time resolution and
280 allows measuring particle- γ -fission coincidences. The combination of SiRi, CACTUS,
281 and NIFF is a powerful setup to investigate the competition of γ decay and fission
282 in highly excited actinide nuclei. By employing charged-particle induced surrogate
283 reactions, such measurements can provide valuable information on neutron-induced
284 reaction cross sections which are not accessible by direct measurements.

285 Acknowledgments

286 Financial support from the University of Oslo for the construction of the detector
287 is gratefully acknowledged. We would also like to thank the staff at the instrumental
288 workshop of the Department of Physics for their help in the manufacture of the parts
289 for the detector and the operators of the Oslo Cyclotron Laboratory for providing the
290 beam. The work has also been supported by the Hungarian OTKA Foundation No. K
291 106035 and by the National Excellence Program TÁMOP 4.2.4.A/2-11-1-2012-0001.

292 References

- 293 [1] J.D. Cramer and H.C. Britt, Nucl. Sci. Eng. **41** (1970) 177.
- 294 [2] J.E. Escher, et al., Rev. Mod. Phys. **84** (2012) 353.
- 295 [3] M. Guttormsen, et al., Phys. Scr. T **32** (1990) 54.
- 296 [4] M. Guttormsen, et al., Nucl. Instr. and Meth. A **648** (2009) 168.
- 297 [5] H. Stelzer, Nucl. Instr. and Meth. A **133** (1976) 409.
- 298 [6] G. Hempel, et al., Nucl. Instr. and Meth. **131** (1975) 445.
- 299 [7] G. Gaukler, et al., Nucl. Instr. and Meth. **141** (1977) 115.
- 300 [8] A. Breskin, et al., Nucl. Instr. and Meth. **144** (1977) 609.
- 301 [9] R. Ganz, et al., Nucl. Instr. and Meth. A **432** (1999) 379.
- 302 [10] J.C. Sanabria, et al., Nucl. Instr. and Meth. A **441** (2000) 525.
- 303 [11] A. Schiller, et al., Nucl. Instr. and Meth. A **447** (2000) 498.